

Deep metric learning for soil organic matter prediction: A novel similarity-based approach using smartphone-captured images

Mojtaba Naeimi ^a, Vishvam Porwal ^b, Stacey Scott ^b, Maja Krzic ^c, Prasad Daggupati ^d, Hiteshkumar Vasava ^a, Daniel Saurette ^e, Ayan Biswas ^f, Abhinandan Roul ^a, Asim Biswas ^{a,*}

^a School of Environmental Sciences, University of Guelph, Guelph, 50 Stone Road East, ON N1G 2W1, Canada

^b School of Computer Science, University of Guelph, 50 Stone Road East, ON N1G 2W1, Canada

^c Department of Forest and Conservation Science, The University of British Columbia, 2357 Main Mall, Vancouver, BC V6T 1Z4, Canada

^d School of Engineering, University of Guelph, 50 Stone Road East, ON N1G 2W1, Canada

^e Ontario Ministry of Agriculture, Food and Agribusiness, 1 Stone Road West, ON N1G 4Y2, Canada

^f Elmore Family School of Electrical and Computer Engineering, Purdue University, 2550 Northwestern Avenue, IN 47906, USA



ARTICLE INFO

Keywords:

Soil Organic Matter
Deep Metric Learning
Triplet Loss
Digital Soil Mapping
Smartphone Sensing
Precision Agriculture
Image Analysis
Machine Learning

ABSTRACT

The accurate assessment of soil organic matter (SOM) is crucial for sustainable agriculture, yet traditional methods remain time-consuming and costly. While smartphone-based digital imaging offers a promising alternative, current approaches face limitations in prediction reliability and generalization capability. This study introduces a novel similarity-based deep learning framework for SOM prediction using smartphone-captured soil images, fundamentally shifting from traditional regression-based methods to a metric learning paradigm. We developed an enhanced image acquisition system and implemented a Triplet Loss network architecture that learns to embed soil images in a semantic space where similarity relationships correlate with SOM content. The system incorporates adaptive image quality assessment and enhancement using the Blind/Referenceless Image Spatial Quality Evaluator and super-resolution techniques. Experimental validation using 500 soil samples from Southern Ontario demonstrated superior performance of our similarity-based approach (validation RMSE = 0.17) compared to traditional regression methods (validation RMSE = 0.51 for Random Forest). The model maintained consistent performance across different soil textures (RMSE variation < 0.05 between texture classes) and environmental conditions (temperature 20–30 °C, humidity 45–75 % RH). The complete analysis pipeline makes the system practical for field applications. Our approach addresses critical challenges in digital soil analysis by providing rapid, reliable, and accessible SOM assessment, contributing to improved soil monitoring and management practices in precision agriculture. These findings demonstrate the potential of similarity-based learning for advancing digital soil sensing technologies and supporting sustainable agricultural practices.

1. Introduction

Climate change presents unprecedented challenges to agricultural sustainability, with soil health playing a pivotal role in adaptation strategies (Zurek et al., 2022). At the core of soil health assessment lies soil organic matter (SOM¹) (Nazir et al., 2024), a critical indicator that influences soil structure, water retention, nutrient cycling, and carbon sequestration (Yan et al., 2023). However, the traditional laboratory-based methods for SOM assessment face significant limitations: they are time-consuming, costly, and often impractical for frequent monitoring needs (M. Aitkenhead et al., 2018; Y. Fan et al., 2021). This

challenge is particularly acute given the dynamic nature of SOM, which can fluctuate significantly over time and space (R. Yang et al., 2022), necessitating rapid and frequent measurements for effective soil management (Qiao et al., 2022; Zeraatpisheh et al., 2022).

The established relationship between SOM and soil color has led to various approaches for SOM estimation, from traditional Munsell color charts to modern digital imaging methods (Tobiszewski & Vakh, 2023). While Munsell charts provided a standardized approach, their subjective nature and non-contiguous color space limit their effectiveness for quantitative analysis (Z. Fan et al., 2017; Gomez-Robledo et al., 2013; Nodi et al., 2023). In practice, these limitations are especially

* Corresponding author.

E-mail address: biswas@uoguelph.ca (A. Biswas).

¹ Soil organic matter.

problematic in agriculture setting where rapid, cost-effective and repeatable soil assessment are essential for timely decision making. Farmers and land managers, particularly those in low-resource environment, require tool that can provide actionable insights without the laboratory testing limitations. As a result, there is an increasing demand for portable, objective and field-adaptable alternatives. Recent advancements suggest that the integration of digital imaging and machine learning holds a substantial promise for accurately predict SOM, especially given the strong visual correlation between soil color and SOM levels (Yang et al., 2024). The use of various color models including red, green, blue (RGB²): hue, saturation, value (HSV³), International Commission on Illumination La*^ab* (CIE La*^ab*⁴), International Commission on Illumination Lu*^v* (CIE Lu*^v*⁵) combined with machine learning approaches, has demonstrated success in capturing this relationship (Azadnia et al., 2022; Babalola et al., 2023).

Building on this potential Kang et al. (2024) showed nonlinear models can exploit color indices, reporting that darker and more yellowish soil were linked to higher SOM, while more saturated colors further improved predictive performance. In addition, combining image and spectral features demonstrated the benefits of dimensionality reduction and showed that convolutional neural network (CNN⁶) outperformed traditional model such as partial least squares regression (PLSR⁷) and support vector machine (SVM⁸) (H. Li et al., 2024). In parallel, efforts have also focused on extending these techniques from controlled laboratory settings to real-world application. Asad et al. (2024) developed a field-ready framework that integrates deep learning with high-resolution ground photography. By using a CNN to segment bare soil regions, followed by machine learning-based SOM prediction, they improved color feature consistency under variable lighting and enabled effective spatial mapping of SOM. This two-step approach highlights the potential of well-designed digital image processing pipeline for rapid, in-situ SOM monitoring.

However, current digital imaging approaches face three critical limitations. First, most studies rely on content-based image retrieval (CBIR⁹) methods that directly map image features to soil properties through regression models (Gozukara et al., 2023). These approaches often struggle with the complex, non-linear relationships between visual features and soil properties. Second, traditional feature extraction methods frequently lose critical color information during color space transformations, leading to reduced prediction accuracy (Gorthi et al., 2021a). Third, existing methods typically treat each image independently, failing to leverage the inherent similarities between soil samples with comparable SOM content.

Recent advances in deep metric learning (DML¹⁰) offer a promising alternative to traditional regression-based approaches (Cheng et al., 2018; Y. Li et al., 2018; Roy et al., 2018). DML techniques, particularly Triplet Loss networks, have demonstrated remarkable success in various computer vision tasks by learning to embed images in a semantic space where similarity relationships are preserved (Hermans et al., 2017). Unlike conventional regression methods, Triplet Loss networks can capture complex visual relationships by considering multiple images simultaneously and learning from their relative similarities (Schroff et al., 2015). This approach is particularly relevant for soil analysis,

where visual similarities often correlate with similar soil properties. While deep learning has revolutionized many areas of agricultural sensing (Waqas et al., 2025), its application to soil property prediction has largely been limited to conventional supervised learning approaches (Table 1). The potential of similarity-based learning, which could better capture the subtle visual relationships between soil samples, remains largely unexplored. This gap is particularly significant given the challenging nature of soil color interpretation, where traditional feature engineering approaches often fail to capture the complex relationships between visual attributes and soil properties.

To address these limitations, this study introduces a similarity-based approach for SOM prediction using smartphone-captured soil images, offering an alternative perspective to existing methods. Our research objectives are to:

Develop and validate a Triplet Loss-based deep learning framework for SOM prediction that leverages image similarities rather than direct regression relationships.

Design an enhanced image acquisition and preprocessing pipeline that preserves critical color information while accounting for variable imaging conditions.

Evaluate the effectiveness of similarity-based learning compared to traditional regression methods across diverse soil conditions and imaging scenarios.

Establish the theoretical and practical advantages of similarity-based approaches for soil property prediction using smartphone imagery.

Together, these objectives aim to explore a shift in digital soil analysis from absolute regression models toward a similarity-learning paradigm.

2. Materials and methods

2.1. Study area and soil sampling

The study was conducted in Southern Ontario within the Boreal Shield and Mixedwood Plains Ecozones, a region that comprises approximately 9 % of Ontario's land area (Fig. 1). Despite its relatively small geographical footprint, this ecozone represents one of the most intensively studied agricultural regions due to its significant agricultural productivity and population density. The region is predominantly characterized by Grey-Brown Podzolic Soils, also known as Grey-Brown Forest Soils.

A total of 500 soil samples were collected from the surface layer (0–15 cm), representing diverse soil textures and organic matter content. The sampling strategy was designed to capture the natural variability in soil properties across the region. After collection, samples were air-dried and sieved according to standard protocols to pass through a 2-mm sieve. Soil organic carbon (SOC¹¹) content was determined using a LECO CN828 Elemental Analyzer, with organic carbon calculated as the difference between total carbon and inorganic carbon. The samples exhibited considerable variation in both textural constituents and organic matter content (Table 2), providing a robust dataset for model development and validation.

2.2. Image acquisition system development

Building upon previous designs (Gorthi et al., 2021a; Gozukara et al., 2023), we developed an advanced imaging chamber specifically optimized for soil color capture. The chamber was 3D printed using matte black material to minimize light reflection and featured multiple adjustable grooves for precise camera positioning. This design addresses a critical limitation in previous studies by enabling consistent image

² Red, Green, Blue.

³ Hue, Saturation, Value.

⁴ International Commission on Illumination L is lightness and a* and b* for the four unique colors: red, green, blue and yellow.

⁵ International Commission on Illumination, L is Lightness, u* is red: green value, v* is yellow: blue value.

⁶ Convolutional Neural Network.

⁷ Partial Least Squares Regression

⁸ Support Vector Machine.

⁹ Content-Based Image Retrieval.

¹⁰ Deep Metric Learning.

¹¹ Soil Organic Carbon

Table 1

Review of smartphone-based Soil Organic Matter (SOM) and Soil Moisture Content (SMS) studies. This table summarizes previous studies, including various models such as Stepwise Multiple Linear Regression (SMLR), Linear Regression (LR), Regression Tree (RT), Support Vector Machine (SVM), Gaussian Process Regression (GPR), Extra Trees (ET), Artificial Neural Networks (ANN), Partial Least Squares Regression (PLSR), Random Forest (RF), Support Vector Regression (SVR), Convolutional Neural Networks (CNN), and Neural Networks (NN).

Input type	Model(s)	Soil property	Number of samples	Prediction accuracy	Region	Reference
Smartphone	SMLR	SOM	25 SMC > 10 %	0.936	4.44 %	Canada
			26 SMC < 10 %	0.819		
Smartphone	LR	SOM	25	0.51	14.21	Canada
		SMC		0.71	11.58	
	RT	SOM		0.54	12.13	
		SMC		0.81	12.73	
	SVM	SOM		0.57	12.35	
		SMC		0.78	10.05	
	GPR	SOM		0.65	10.64	
		SMC		0.84	10.65	
	ET	SOM		0.73	9.64	
		SMC		0.81	9.9	
	Other/ANN	SOM		0.91	5.45	
		SMC		0.75	9.89	
Smartphone	image morphometrics	SOM	103			Scotland
Smartphone	SMLR/PLSR	SOM	70	0.68–0.77	5.32–7.12	China
Smartphone	RF/ SVR/ AdaBoost/Regression/ Ridge	SOM	90	RI ^a - 0.88 PI ^b - 0.79	0.28 0.36	India
Smartphone	NN PLS	SOM	273		1.6 1.9	Ethopia
Smartphone	RF	SOC	611	0.42–0.7		Turkey
Smartphone	CNN	SOM	20	accuracy > 99 %		Turkey

^a Reflectance Image.

^b Perpetuated Image.

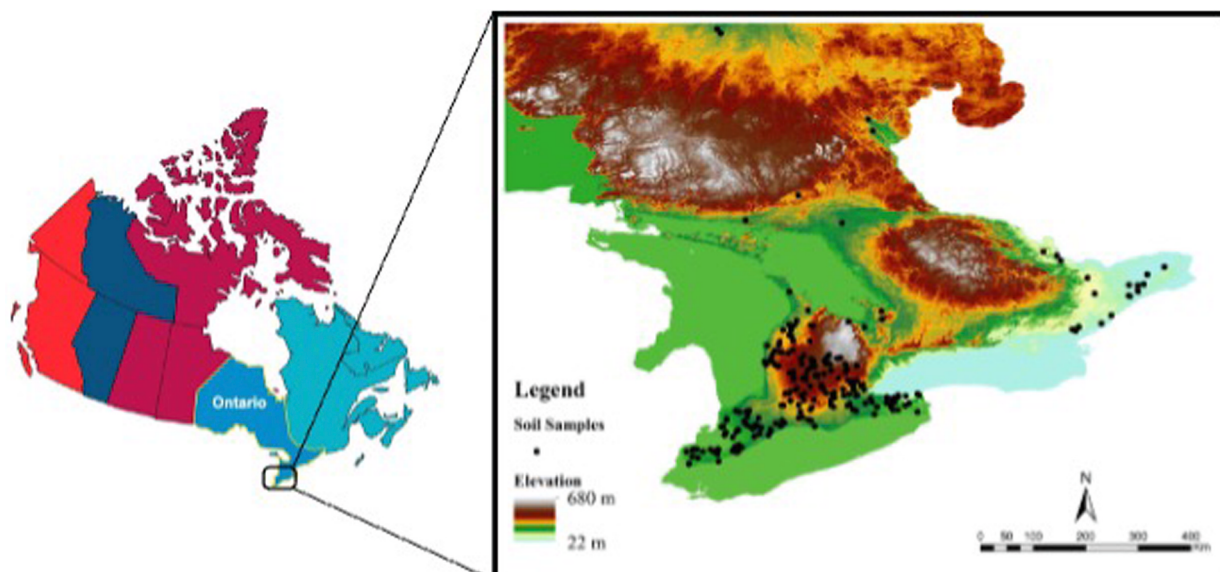


Fig. 1. Overview of the Study Area in Southern Ontario: The green rectangle highlights the study area within Southern Ontario, while the red points on the digital elevation model indicate the sample locations. These locations are primarily associated with Grey-Brown Forest Soils.

Table 2

Textural constituents and organic matter distribution data.

Statistics	Textural constituent			SOM
	Clay	Silt	Sand	
Mean	27.40	36.45	36.14	2.10
Median	25.00	37.90	31.00	2.04
Maximum	73.20	92.70	93.50	14.10
Minimum	4.10	1.60	2.10	0.47

capture geometry while maintaining uniform illumination conditions (Fig. 2).

The illumination system was calibrated to 500 lx using an Extech LT505 light meter, with regular recalibration performed every 10 samples to maintain consistency. Light was incident at a 45-degree angle to minimize specular reflection, and a fixed 10 cm distance was maintained between the sample and camera for optimal field of view. Images were captured using an iPhone 14 Pro at 3024 × 4032 pixel resolution and saved in JPEG format. Each soil sample was placed in a standardized Petri dish within the imaging chamber, and images were subsequently cropped to 1000 × 1000 pixels from the center to eliminate peripheral distortions.



Fig. 2. 3D-printed chamber for soil image-acquisition. The left image shows the chamber connected to its power source, featuring a ceiling-mounted LED light system managed via a mobile application to provide adjustable illumination settings. The right image displays the chamber with the door removed, revealing the adjustable-height tray and a soil sample in a Petri dish placed on top.

2.3. Image processing and feature extraction

A comprehensive image processing workflow was implemented to maximize the quality and reliability of soil color information (Fig. 3). The process began with conversion to grayscale using the luminosity method, which applies channel-specific weights ($0.2989R + 0.5870G + 0.1140B$) to preserve perceptual luminance relationships. Global histogram equalization was then applied using a 256-bin histogram, enhancing image contrast while maintaining the relative distribution of intensity values. This step proved crucial for standardizing images captured under slightly varying conditions, particularly in compensating for minor illumination fluctuations.

Noise reduction was achieved through a two-stage filtering process. First, a Gaussian filter with a 5×5 kernel size and $\sigma = 1.0$ was applied to reduce high-frequency noise while preserving edge information. This was followed by bilateral filtering (spatial $\sigma = 75$, intensity $\sigma = 75$, kernel size = 9) to further reduce noise while maintaining important edge transitions that often correspond to soil structural features. Local contrast enhancement was then performed using adaptive histogram equalization (AHE¹²), with the image divided into 8×8 tiles and contrast limiting (CLAHE¹³) applied with a clip limit of 2.0 to prevent over-amplification of noise in homogeneous regions.

The optimized threshold-based segmentation utilized an intensity range of 0.2–0.8, determined through extensive experimentation to provide optimal separation between soil regions and potential artifacts. The resulting binary mask underwent a series of morphological operations, including opening (3×3 kernel) to remove small noise artifacts, closing (5×5 kernel) to fill small holes, and area-based filtering to remove regions smaller than 100 pixels. This refined segmentation mask was then applied to the original image to isolate the soil region for subsequent analysis.

Following segmentation, we implemented a comprehensive color space transformation pipeline to capture both device-dependent and perceptually uniform color characteristics (Table 3). Images were transformed from the native RGB color space to HSV for intuitive color

representation, CIE La*b* for perceptual uniformity, and CIE Lu*v* for enhanced chromaticity discrimination (Cheung & Rhodes, 2023; Hema & Kannan, 2019). From these transformed images, we extracted a carefully selected set of 17 features (Fig. 4), including statistical measures (mean, median, standard deviation) and specialized color indices (Table 3). These indices, including the Redness Index, Coloration Index, Hue Index, and Brightness Index, were specifically chosen based on their demonstrated relationships with SOM content in previous research.

2.4. Development of prediction models

The cornerstone of our approach is the design of a Triplet Loss network architecture for SOM prediction, contributing a new dimension of image-based soil analysis. The network architecture (Fig. 5) consists of three identical convolutional neural networks that share weights, designed to process image triplets consisting of an anchor image, a positive image (same sample with on-the-fly augmentations such as random horizontal flip and brightness/contrast jitter), and a negative image was selected deterministically as the sample whose SOM value differed most from the anchor (Fig. 6). This design enforces strong semantic separation in each triplet and enables the network to learn relative relationships between soil samples rather than absolute mappings, potentially capturing more nuanced relationships between visual features and organic matter content.

The network implementation utilized a ResNet-50 backbone, pre-trained on ImageNet and modified for soil-specific feature extraction. The model architecture incorporates several deliberate design elements: a modified first convolution layer optimized for soil features, intermediate feature maps preserved at multiple scales, and skip connections maintained for robust gradient flow. Global average pooling was employed for feature map aggregation, producing fixed-length feature vectors that undergo L2 normalization before Triplet Loss computation. Training was conducted for 10 epochs with a batch size of 64 using the Adam optimizer (learning rate = 2×10^{-5}) on a CUDA-enabled GPU. A cosine-similarity-based Triplet Loss (margin = 1.0) guided optimization. Model weights were checkpointed every five epochs, with validation loss monitored to guard against overfitting, and gradient clipping at a norm of 1.0 was applied to ensure stable training.

Prior to training, we implemented a comprehensive quality

¹² Adaptive Histogram Equalization

¹³ Contrast Limiting Adaptive Histogram Equalization

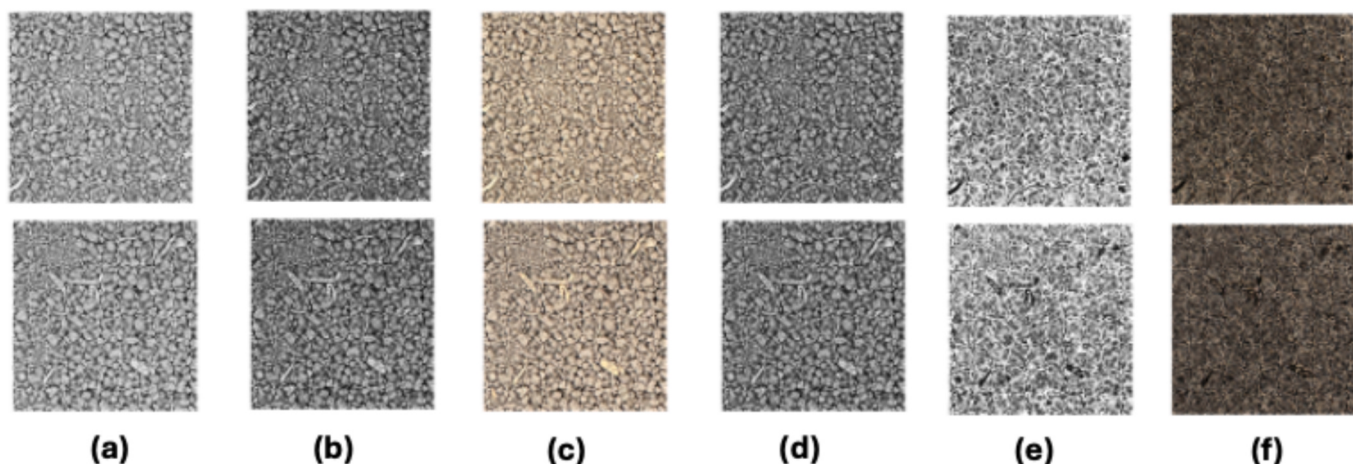


Fig. 3. Image Processing Steps for Soil Sample Analysis. This figure demonstrates the sequential steps applied in the image processing workflow, illustrated with two example soil samples. (a) The grayscale conversion of the original image; (b) the equalized image to enhance contrast; (c) the application of Gaussian filtering to reduce noise; (d) adaptive histogram equalization for localized contrast enhancement; (e) the segmentation mask generated for isolating the region of interest; and (f) the final segmented image highlighting the soil sample.

Table 3

Color Models and Parameters for Soil Analysis: Comparison of color model spaces (RGB, HSV, CIE La^{*}b^{*}, and CIE Lu^{*}v^{*}) with descriptions and applications relevant to soil color analysis and property prediction.

Color Space	Color Feature	Description	Significance
RGB	R	one primary color with primary stimulus occurring at 700 nm, combination of lightness and chromaticity (hue and chroma)	Represents soil redness; can be correlated with organic matter or iron oxide content.
	G	one primary color with primary stimulus occurring at 546 nm, combination of lightness and chromaticity (hue and chroma)	Useful for assessing green hues, often indicative of vegetation or moisture.
	B	one primary color with primary stimulus occurring at 436 nm, combination of lightness and chromaticity (hue and chroma)	Indicates soil blueness; can help differentiate soil types under specific lighting.
HSV	H	hue, $H = (2G - R - B)/4$	Represents the dominant color perceived; helps identify soil type and composition.
	S	$S = V - \max(R, G, B) / V$, where $V = \max(R, G, B)$	Useful for analyzing soil chromaticity and its moisture levels.
CIE La [*] b [*]	V	$V = \max(R, G, B)$	Indicates brightness, useful for assessing soil reflectance and lighting conditions.
	L	lightness, range from black to white	Helps in assessing soil image brightness
	a [*]	chroma, redness (positive a [*]) or greenness (negative a [*])	Effective for quantifying soil color's red-green balance
CIE Lu [*] v [*]	b [*]	chroma, yellowness (positive b [*]) or blueness (negative b [*])	Used for yellow-blue balance, often related to soil mineral content.
	L	lightness, range from black to white	As in Lab, critical for lightness differentiation in soil imaging.
	u [*]	chroma, redness (positive u [*]) or greenness (negative u [*])	Used for red-green chromatic analysis, providing insights into soil pigmentation.
	v [*]	chroma, yellowness (positive v [*]) or blueness (negative v [*])	Complements b [*] in Lab, offering more perceptually uniform chromatic insights.

assessment and enhancement system (Zhao et al., 2024) to ensure robust performance across varying image qualities. Using OpenCV's dnn_sperres and scikit-image, blind/referenceless image spatial quality evaluator (BRISQUE¹⁴) was configured specifically for soil imagery, with feature extraction optimized for soil-specific characteristics. Each image was first denoised via BayesShrink wavelet thresholding in YCbCr space, then assigned a pre-enhancement BRISQUE score to quantify image quality. Images falling below our quality threshold underwent adaptive super-resolution enhancement (Fig. 7), utilizing a modified super-resolution convolutional neural network (SRCNN¹⁵) architecture with soil-specific layers and dynamic upscaling factor determination based on input quality. Finally, we recorded a post-enhancement BRISQUE score, and only enhanced images were passed on to model training.

For comparative evaluation, we implemented five traditional machine learning models, each configured with optimized parameters

determined through rigorous cross-validation. The Random Forest (RF¹⁶) model utilized 500 trees with optimized maximum depth, while the SVM employed a radial basis function kernel with parameters determined through grid search optimization. The PLSR implementation used the non-linear iterative partial least squares algorithm and to select the optimal number of latent components, models evaluated with 1–10 components via five-fold cross-validation on the training set, while both multivariate linear regression (MLR¹⁷) and stepwise multiple linear regression (SMLR¹⁸) models incorporated comprehensive condition number checking and residual analysis. Feature inclusion and exclusion were governed by OLS p-value, with an entry threshold of 0.01 and exit threshold of 0.05, starting from an intercept-only model.

All models underwent training using a 70–30 split for calibration and validation datasets, maintained consistently across experiments through fixed random seed initialization. Performance evaluation utilized

¹⁴ Blind/Referenceless Image Spatial Quality Evaluator.

¹⁵ Super-Resolution Convolutional Neural Network.

¹⁶ Random Forest.

¹⁷ Multivariate Linear Regression

¹⁸ Stepwise Multiple Linear Regression

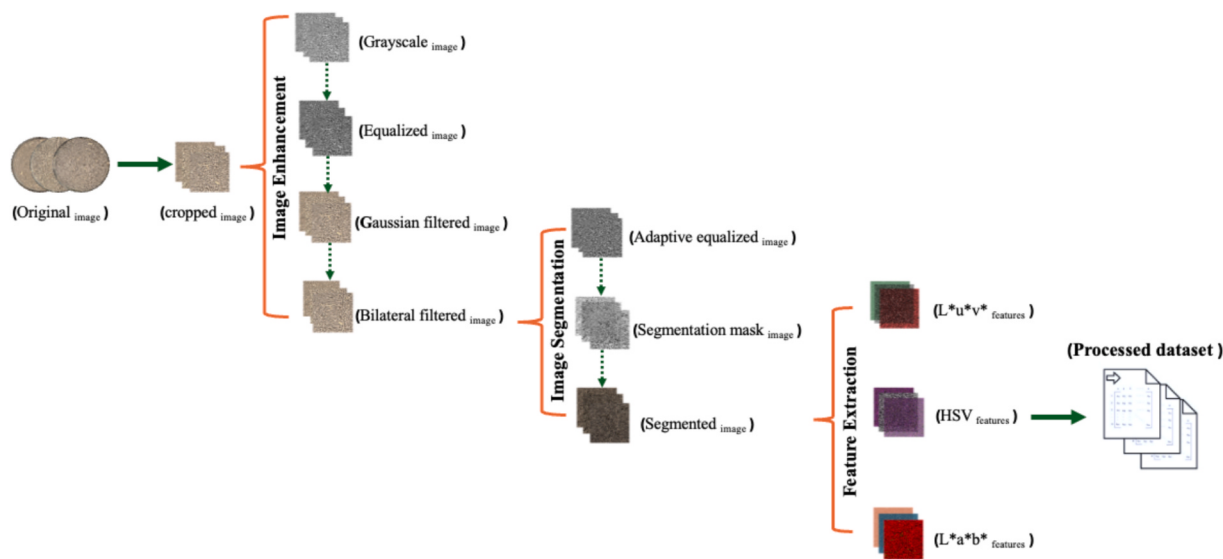


Fig. 4. Workflow for Image Processing and Feature Extraction. The figure outlines the steps from raw digital soil sample images to a processed dataset. The process starts with raw digital image, followed by a series of image processing steps (as detailed in Fig. 3). Finally, feature extraction is performed on the segmented images, analyzing color properties in HSV, CIE La^{*}b^{*}, and CIE Lu^{*}v^{*} color spaces to generate a structured dataset for further analysis.

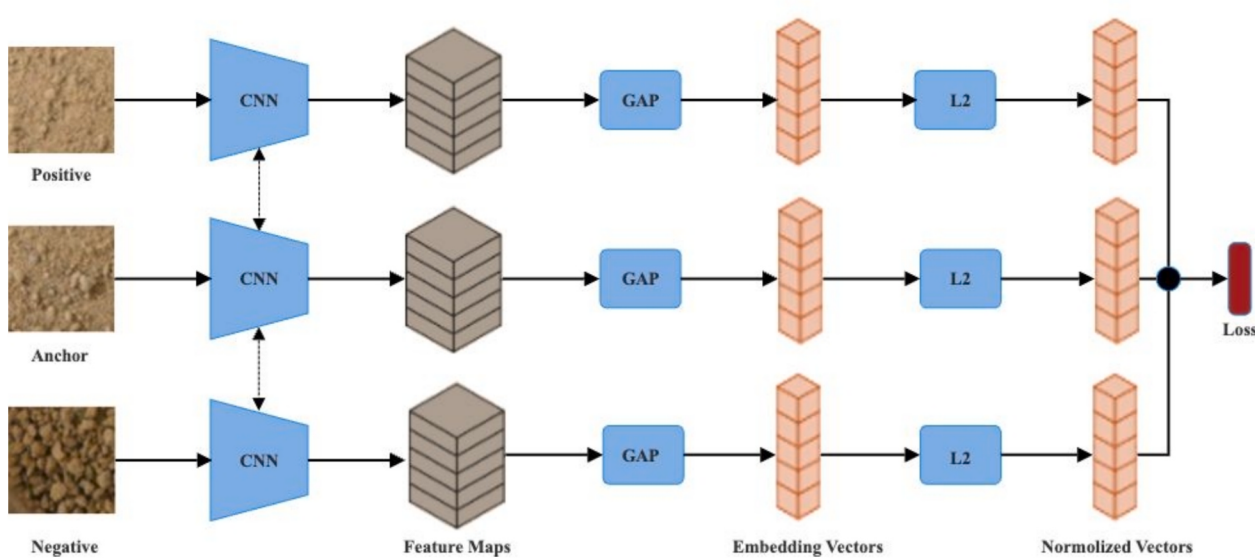


Fig. 5. Triplet Network Architecture for Soil Organic Matter (SOM) Analysis. The architecture features three identical convolutional neural networks (CNNs) with shared weights, designed to process image triplets: an anchor image, a positive image (similar SOM content), and a negative image (different SOM content). Feature maps are extracted, passed through Global Average Pooling (GAP) layers and L2 normalization, and compared using a triplet loss function to optimize the network's ability to distinguish soil samples based on SOM content.

multiple complementary metrics including RMSE,¹⁹ MSE,²⁰ and MAE.²¹ Statistical significance of performance differences was assessed through paired t-tests with Bonferroni correction for multiple comparisons, complemented by effect size calculations using Cohen's d to quantify practical significance. To validate the Triplet Loss embedding and to interpret its inner working, first we applied a 3D Uniform Manifold Approximation and Projection (UMAP)²² to confirm that the feature space can capture SOM as a continuous gradient, then to quantify each embedding dimension's contribution to SOM prediction, we trained a

Ridge regressor on the embeddings using KernelSHAP. To understand what the key color coordinates in each embedding are, we merged each image's embedding values with its original color coordinates to correlate the top embedding dimensions with physical features. Finally, an external validation was conducted on unseen data, using an independent dataset from a farmland in New Brunswick, Canada to evaluate the reliability and generalizability of the Triplet Loss model. Analyses were conducted using both Python and R.

3. Results

3.1. Performance analysis of color features and soil properties

The analysis of color parameters revealed significant correlations

¹⁹ Root Mean Square Error.

²⁰ Mean Square Error.

²¹ Mean Absolute Error.

²² Uniform Manifold Approximation and Projection

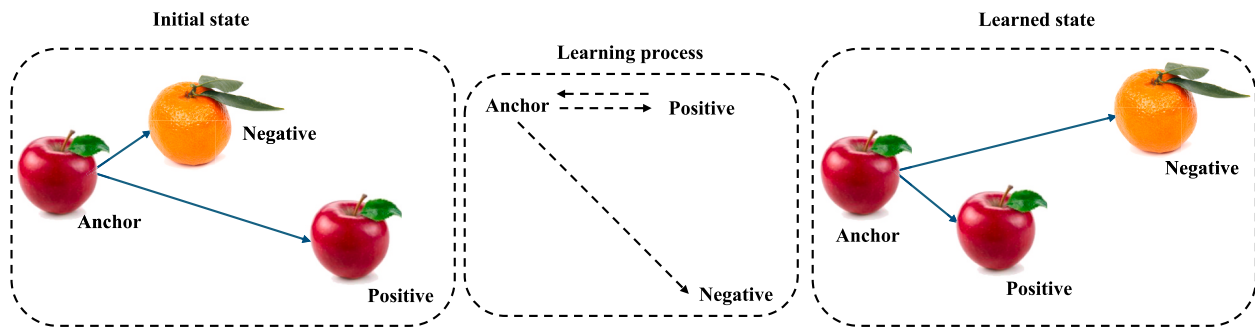


Fig. 6. Triplet Loss Training Mechanism. This figure illustrates the triplet loss training process, where an anchor image is compared with a positive image (similar) and a negative image (dissimilar). During training, the distance between the anchor and positive images ($d(a, p)$) is minimized, pulling the positive closer to the anchor. Simultaneously, the distance between the anchor and negative images ($d(a, n)$) is maximized, pushing the negative further away.

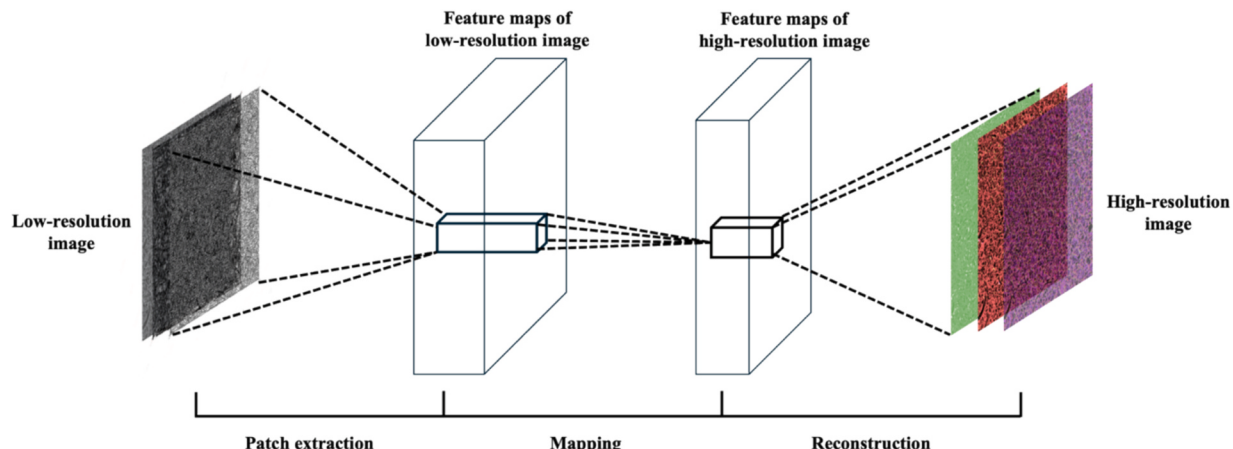


Fig. 7. Super-Resolution Workflow for Soil Image Enhancement. This figure illustrates the process of applying super-resolution techniques to enhance soil image quality. Transforming low-resolution image (left) into a high-resolution output (right) using a neural network.

pattern, as shown in Fig. 8. Red (R) and Green (G) channels demonstrated strong positive correlations ($r = 0.918$), while Blue (B) showed moderate correlation with both R ($r = 0.632$) and G ($r = 0.877$). In the CIE Lab color space, the L parameter exhibited strong correlations with

RGB values ($r > 0.838$), indicating its effectiveness in capturing soil brightness variations. The u^* and v^* parameters in CIE Lu^*v^* space showed strong correlations with a^* and b^* parameters ($r > 0.781$), suggesting redundancy in chromaticity information across color spaces. These correlations provide fundamental support for the use of multiple color spaces in SOM prediction.

3.2. Comparative analysis of regression and Similarity-Based models

The performance of traditional regression models and the similarity-based Triplet Loss approach was evaluated across both calibration and validation phases (Table 4). During calibration, the RF model

Table 4

Model Performance Metrics. Comparison of MSE, RMSE, and MAE for different models during calibration and validation phases, including Random Forest, Support Vector Machine, Partial Least Squares Regression, Multivariate Linear Regression, Stepwise Multiple Linear Regression, and Triplet Loss.

Model	Calibration			Validation		
	MSE	RMSE	MAE	MSE	RMSE	MAE
Random Forest	0.04	0.20	0.16	0.26	0.51	0.41
Support Vector Machine	0.22	0.46	0.35	0.30	0.55	0.43
Partial Least Squares Regression	0.24	0.49	0.39	0.28	0.53	0.42
Multivariate Linear Regression	0.23	0.48	0.37	0.30	0.55	0.44
Stepwise Multiple Linear Regression	0.27	0.52	0.41	0.25	0.50	0.40
Triplet loss	0.10	0.32	0.27	0.03	0.17	0.14

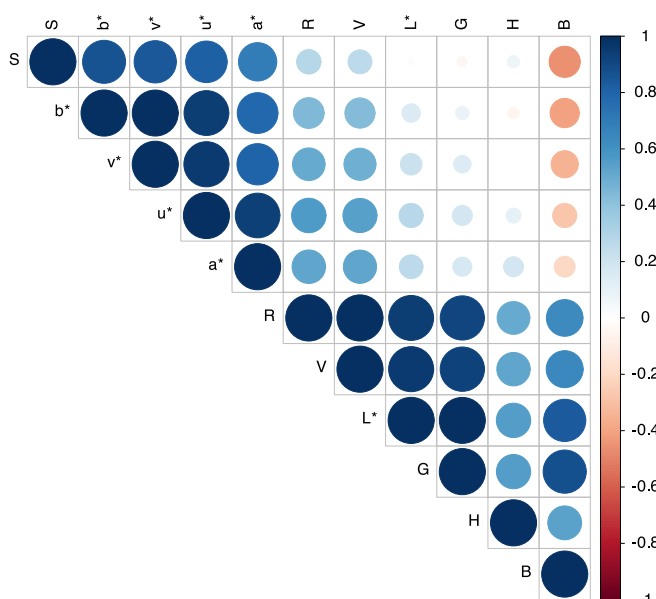


Fig. 8. Correlation Plot of Color Parameters Across Different Color Models.

outperformed others, achieving the lowest error metrics ($MSE = 0.04$, $RMSE = 0.20$, $MAE = 0.16$), followed by SVM, while PLSR, MLR, and SMLR showed higher error rates (MSE ranging from 0.23 to 0.27). However, all regression models exhibited a notable drop in performance during validation. The RF model, despite its strong calibration results, experienced the most significant degradation (validation $RMSE = 0.51$), suggesting possible overfitting, even after cross-validation optimization.

In contrast, the Triplet Loss model demonstrated remarkable stability between calibration and validation phases. During calibration, it achieved moderate performance ($MSE = 0.10$, $RMSE = 0.32$, $MAE = 0.27$), but notably maintained superior performance during validation ($MSE = 0.03$, $RMSE = 0.17$, $MAE = 0.14$), indicating better generalization across diverse soil types and imaging conditions. This stability highlights its potential as a more robust alternative to traditional regression approaches. Furthermore, the Triplet Loss training process converged efficiently, with the loss function stabilizing within 30 epochs (Fig. 9), and training MSE showing consistent decline. This relatively quick convergence indicates efficient learning of meaningful soil image representations.

Direct comparison between the Triplet Loss model and the best-performing regression model, RF, reveals significant differences in prediction stability. Fig. 10 illustrates this comparison, showing the Triplet Loss model's superior performance particularly in the validation phase. While the RF model showed stronger performance during calibration, its significant degradation during validation ($RMSE$ increase from 0.20 to 0.51) contrasts sharply with the Triplet Loss model's improved validation performance ($RMSE$ decrease from 0.32 to 0.17). Statistical analysis of the performance differences confirmed the significance of these results ($p < 0.01$). The Triplet Loss model showed particularly strong performance in predicting SOM values between 2–5 %, which represents the most common range in agricultural soils of the study region. This suggests practical advantages for routine soil monitoring applications.

3.3. Effects of image quality enhancement and soil texture

The implementation of the BRISQUE-based quality assessment and enhancement system demonstrated measurable improvements in prediction accuracy. Images identified as low-quality (BRISQUE score > 45) showed an average improvement of 23 % in prediction accuracy after enhancement through our super-resolution pipeline (Fig. 11). This improvement was particularly notable in challenging imaging conditions, such as samples with high surface roughness or variable moisture content. Beyond image quality, soil texture also plays a crucial role in prediction accuracy. Analysis of model performance across varying soil textures revealed important patterns in prediction accuracy. The Triplet Loss model maintained consistent performance across different texture classes, with RMSE variations of less than 0.05 between clay, loam, and sandy soil types. In contrast, regression models showed greater

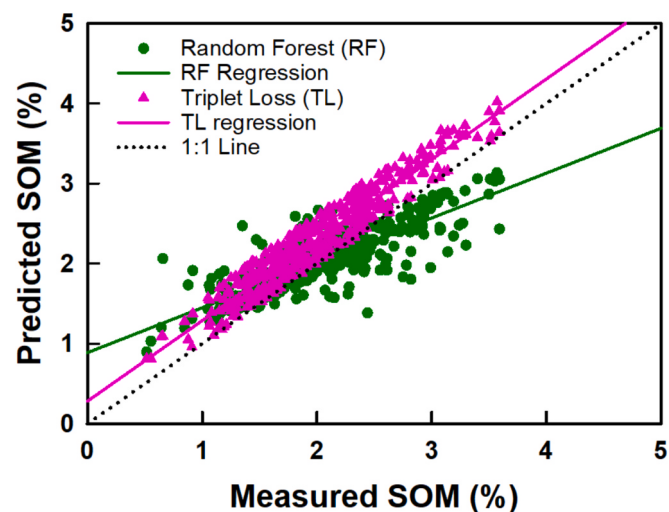


Fig. 10. Comparison of Predicted vs. Measured Soil Organic Matter (SOM) Using Random Forest and Triplet Loss Models. The scatterplot compares the predicted SOM values (%) with the measured SOM values (%) for two modeling approaches: Random Forest (RF) and Triplet Loss (TL). Green circles represent RF predictions, while magenta triangles represent TL predictions. Solid lines indicate regression trends for RF and TL models, with the dotted line representing the ideal 1:1 agreement.

sensitivity to soil texture, with RMSE variations up to 0.15 between texture classes. The RF model, while effective overall, showed reduced accuracy in clay-rich soils ($RMSE = 0.58$ for samples with $> 50\%$ clay content) compared to medium-textured soils ($RMSE = 0.41$).

3.4. Model reliability analysis and computational performance

The 3D UMAP reveals a continuous gradient along specific directions in the embedding space, indicating SOM values are organized meaningfully (Fig. 12). This suggests that the Triplet Loss effectively guided the network to cluster images based on SOM similarity. The smooth transitions further demonstrate that the learned distance metric captures a roughly continuous relationship between image appearance and SOM content. The UMAP shows the entire space is organized by SOM, but it does not show the contributions of each embedding in SOM prediction, while SHAP analysis exactly shows which embeddings are the most important ones in SOM prediction. Fig. 13 shows the most important embeddings contributions and Fig. 14 shows the image feature importance in top 5 embeddings. The error distribution analysis revealed distinct patterns in prediction accuracy across different SOM ranges. The Triplet Loss model demonstrated normally distributed errors across the full spectrum of SOM values, as confirmed by the Shapiro-Wilk test ($p >$

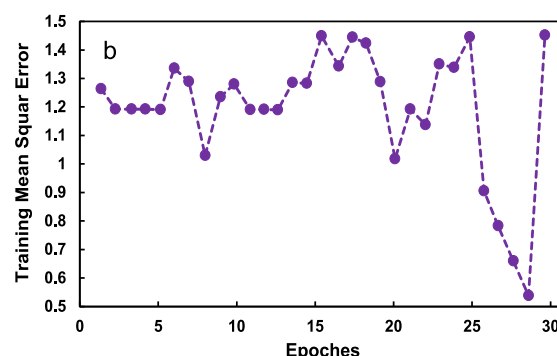
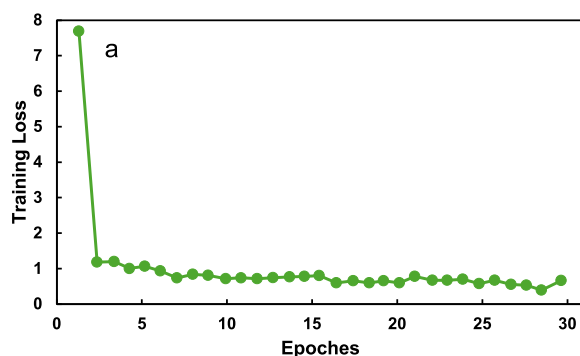


Fig. 9. Training Progression for the Model. The left plot shows the training loss over 30 epochs, indicating a rapid decrease in loss during the initial epochs, followed by stabilization, reflecting model convergence (a). The right plot presents the training mean squared error (MSE) over the same epochs, illustrating fluctuations during training with a notable drop toward the end (b).

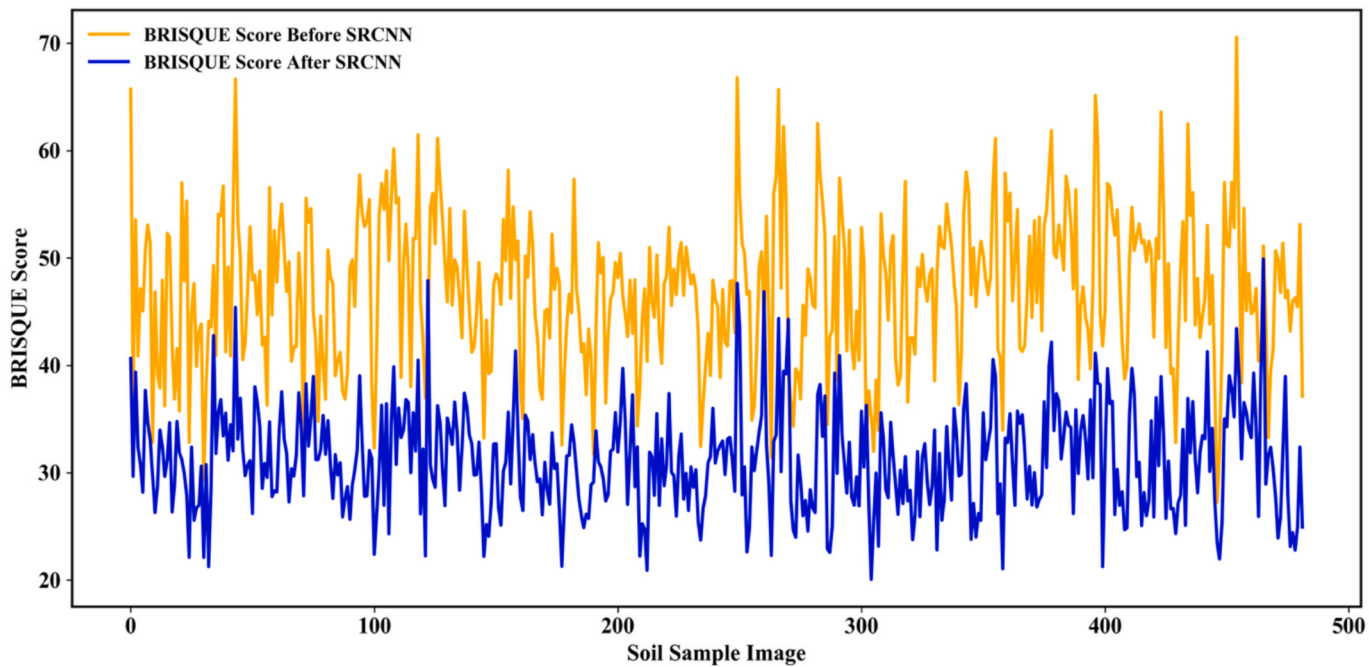


Fig. 11. BRISQUE-based image quality assessment before and after super resolution enhancement using SRCNN for 500 soil image samples. The orange line represents the original BRISQUE scores, while the below line shows the scores after enhancement.

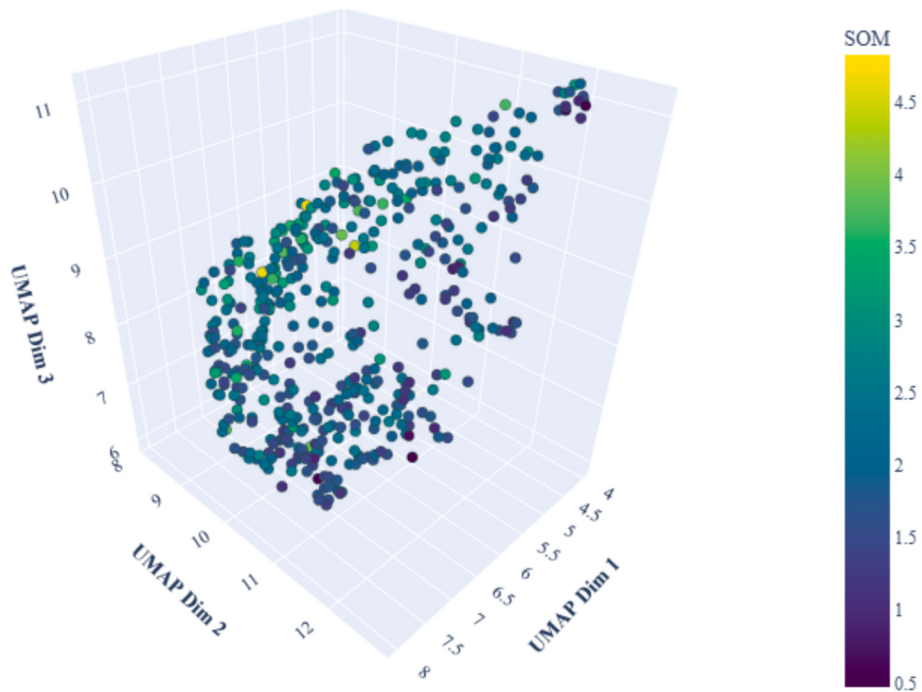


Fig. 12. The 3D UMAP projection of the 128-D Triplet Loss embeddings, colored by measured SOM. The smooth gradient from purple (low SOM) to yellow (high SOM) demonstrates that the learned embedding space retains a continuous SOM signal.

0.05). This consistent error distribution suggests reliable performance across different soil conditions. In contrast, regression models exhibited heteroscedastic behavior, with error variance increasing notably at higher SOM values. This pattern was particularly pronounced for samples with SOM content exceeding 8 %, where regression models showed a systematic tendency to underestimate SOM levels. The RF model, despite its overall strong performance, exhibited similar bias at high SOM values, suggesting a fundamental limitation in the regression-based approach to extreme values.

Additional analysis of prediction reliability across different soil textures revealed that the Triplet Loss model maintained consistent performance regardless of soil texture classification. The model's error metrics showed minimal variation across clay, loam, and sandy soil types, with RMSE variations not exceeding 0.05 between texture classes. This stability across different soil textures represents a significant advantage over traditional regression approaches, which showed texture-dependent performance variations up to three times larger. Such consistency in performance across diverse soil conditions suggests that

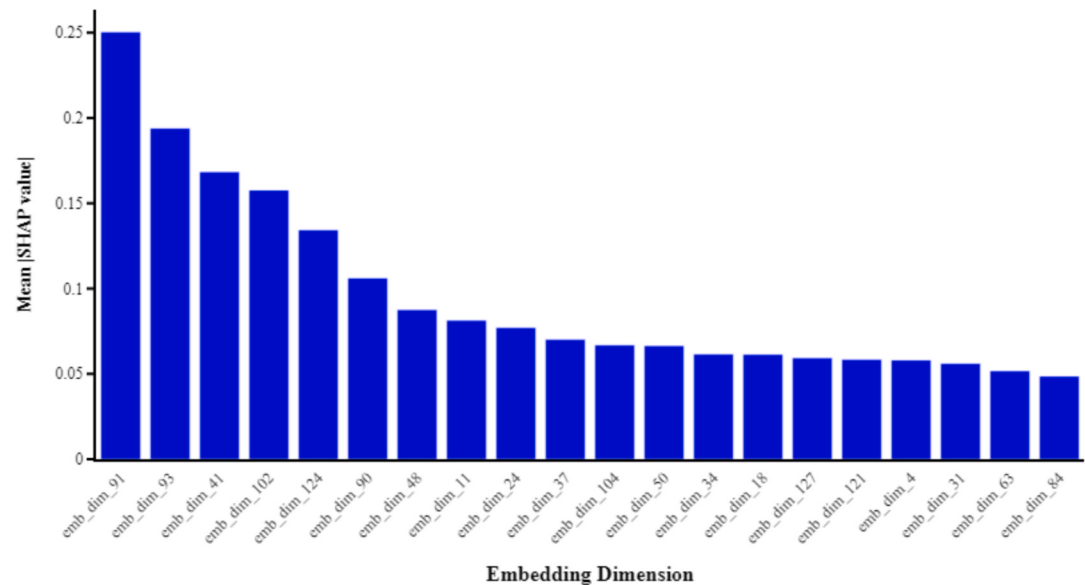


Fig. 13. Mean absolute SHAP value for each embedding dimension, computed via KernelSHAP on a Ridge regressor. The most influential dimensions have mean |SHAP| > 0.1, whereas almost 100 dimensions contributed negligibly.

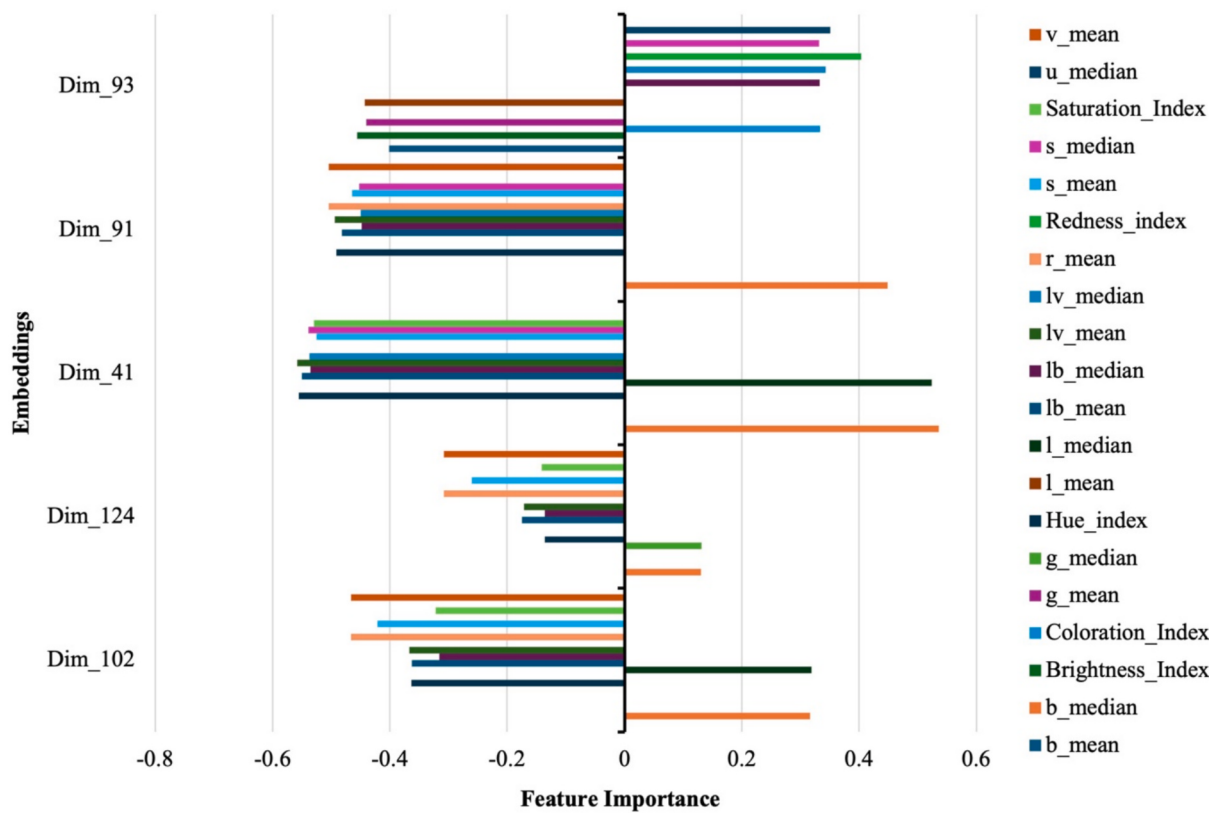


Fig. 14. Feature importance across the top five embedding dimensions, highlighting contributions from HSV, La*b* and Lu*v* and derived color indices. Notable contributors include b_median, Hue_index and lb_mean, with varying strength and direction of association.

the similarity-based approach better captures the fundamental relationships between soil visual properties and organic matter content, independent of confounding textural variations. Processing time analysis revealed important practical considerations for field implementation. The complete processing pipeline, including image preprocessing, enhancement, and prediction, required approximately 2.3 s per sample on standard computing hardware (Intel i7 processor, 16 GB RAM).

Image preprocessing and enhancement consumed most of this time at 1.2 s, followed by feature extraction at 0.8 s. The prediction phase showed varying computational demands across models, with the Triplet Loss model requiring 0.3 s, while the RF model completed predictions in 0.1 s. Other regression models demonstrated even faster prediction times, completing their analyses in less than 0.1 s. Although the Triplet Loss model demanded slightly more computational resources, the total

processing time remains well within acceptable limits for practical field applications, especially considering the improved prediction accuracy and stability.

3.5. Environmental and feature Effects on stability and Interoperability in SOM prediction

To assess the practical robustness of our approach, we conducted repeated measurements of 50 selected samples under varying environmental conditions over a one-week period. The Triplet Loss model demonstrated remarkable temporal stability, maintaining prediction accuracy with a coefficient of variation of 4.2 % across repeated measurements. Temperature variations (20–30 °C) and ambient humidity changes (45–75 % RH) had minimal impact on prediction accuracy (RMSE variation < 0.03), suggesting robust performance under typical field conditions. Beyond environmental stability analysis of feature contributions in the regression models revealed interesting patterns in the relative importance of different color parameters. In the RF model, the L parameter from CIE La*b* space showed the highest importance score (0.28), followed by the Redness Index (0.21) and b* parameter (0.19). The HSV color space parameters showed relatively lower importance scores (H: 0.12, S: 0.14, V: 0.15), suggesting that perceptually uniform color spaces might be more informative for SOM prediction. Further evaluating model stability, cross-validation results highlighted the model stability across different data partitions. The Triplet Loss model showed the most consistent performance across all 10 folds, with a standard deviation in RMSE of 0.023, compared to 0.047 for RF and 0.062 for SVM. This consistency was particularly evident in the prediction of extreme SOM values (<1% and > 10 %), where traditional models often showed increased variability. An analysis of top 5 embeddings dimensions revealed consistent contribution from multiple color spaces. In the RGB color space, b_median contributed to 4 of the 5 dimensions. From HSV, s_mean showed strong influence (0.26–0.52), while from RBG-based color indices, Hue_index had the highest single contribution (0.56 in Dim_41). The CIE-based color spaces, La*b* and Lu*v* showed the most consistent contributions, especially from the b-axis parameters (lb_mean, lb_median), which appeared across all five dimensions with values ranging from 0.13 to 0.54. Lightness value, L parameter, also contributed meaningfully. Among the color indices, Hue_index and Saturation_index were the most influential, contributing to 4 and 3 dimensions respectively. In contrast, Redness, Coloration and Brightness indices, each contributed to only one dimension. These findings highlight the importance of perceptually-uniform and hue-based features in shaping the embedding space.

3.6. External validation on an independent dataset

To assess the robustness and generalizability of the Triplet Loss model beyond the original study area, we conducted an external validation using an independent dataset collected from an agricultural field in New Brunswick, Canada. A total of 40 soil samples were collected, imaged under the same conditions, and analysed in the laboratory for reference SOM content. When the trained model was applied to this dataset, it achieved a RMSE of 0.49 %, and a MAE of 0.41 %. The measured SOM values in the external dataset ranges from 1.69 % to 2.8 %, while predictions spanned from 0.99 % to 2.7 %. The scatter around the regression line remained relatively uniform across the 1–3 % SOM range, with no obvious increase in error at either extreme (Fig. 15). When challenged with a completely independent dataset, the Triplet Loss model achieved a lower RMSE (0.49 %), then all five traditional algorithms, outperforming even their internal validation results which ranged from 0.50–0.55 %. These results demonstrate that the model is transferrable to different climate zones and soil parent material, supporting its potential for broader application. Future work should explore field-based image acquisition, under variant moisture and ambient lighting conditions, as well as additional land use type, to further

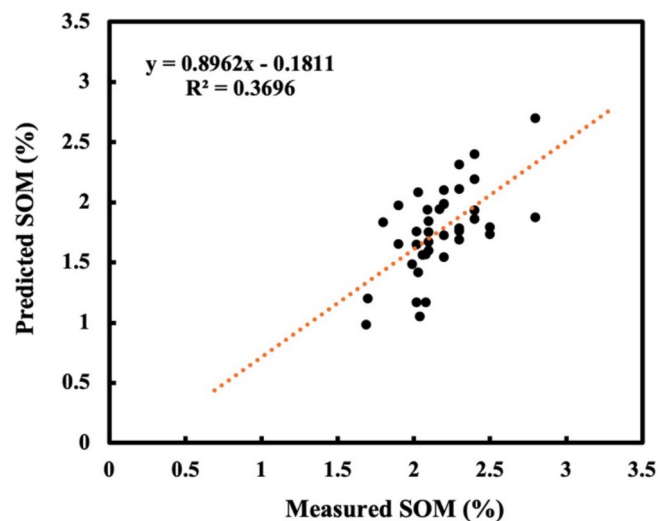


Fig. 15. External validation of the Triplet Loss model on an independent dataset from New Brunswick.

strengthen the model's applicability in real-world farming scenarios.

4. Discussion

The development and validation of our similarity-based approach for SOM prediction represents a significant advancement in digital soil analysis, addressing key limitations of traditional methods while opening new possibilities for rapid, in-situ soil assessment using smartphone imagery.

4.1. Comparative advantages of Similarity-Based learning

The superior validation performance of the Triplet Loss model ($\text{RMSE} = 0.17$) compared to traditional regression models (e.g., $\text{RMSE} = 0.51$ for RF) highlights a core strength of the similarity-based learning paradigm. While conventional regression models such as RF and SVM achieved strong calibration results, their marked decrease in validation performance suggests limited generalizability and limitations in capturing the complex relationships between soil visual properties and organic matter content. This observation is consistent with previous studies by Gozukara et al. (2023), who noted that traditional regression approaches often struggle with the non-linear relationships inherent in soil color-property relationships.

The stability of the Triplet Loss model's performance between calibration and validation phases (RMSE improvement from 0.32 to 0.17) represents a crucial advancement over previous smartphone-based approaches. This finding aligns with recent criticisms of traditional regression models' sensitivity to complex, non-linear relationships between visual features and SOM content (Fu et al., 2020; Taneja et al., 2021). Our results suggest that by learning to compare soil samples rather than directly mapping features to SOM values, the Triplet Loss model develops more robust and generalizable representations of soil properties.

It is important to note that, rather than training the Triplet Loss architecture to directly predict Soil Organic Matter (SOM) through regression, we adopted a two-stage approach that first learns a compact, discriminative embedding space. In this space, images with similar visual patterns and SOM levels are positioned closer together, while those with dissimilar characteristics are pushed further apart. Once the embedding model is trained, SOM prediction is achieved by retrieving the top 5 most similar samples in the embedding space using an Annoy-based approximate nearest neighbor search. The final SOM value for a test image is then inferred as the average SOM of these retrieved

neighbors. This method allows us to decouple the representation learning from the regression task, improving the model's interpretability and robustness under varying imaging conditions. It also facilitates the integration of field-acquired images in future deployments, as the retrieval-based approach is less sensitive to domain shift than direct regression models. The application of Triplet Loss in this study offers distinct advantages for soil image analysis, particularly in addressing the variability inherent in soil color, texture, and imaging conditions. Unlike conventional regression models, which often struggle with generalization when exposed to heterogeneous field data, the Triplet Loss framework learns a structured embedding space that captures perceptual similarity aligned with SOM variation. This is especially important in soil contexts, where small changes in surface moisture, illumination, or aggregation can drastically alter visual appearance despite similar organic matter content. By learning relative relationships between samples, rather than absolute values, Triplet Loss provides a robust mechanism to accommodate such inconsistencies.

4.2. Environmental robustness and practical Utility

Environmental variability often hinders the consistency of smartphone-based soil analysis, but our approach showed promising resilience. The Triplet Loss model maintained high predictive accuracy across a range of temperatures (20–30 °C) and humidity levels (45–75 % RH), with an RMSE variation of less than 0.03. Temporal robustness was also evident, with repeated measurements across a week yielding a low coefficient of variation (4.2 %). Moreover, the integration of BRISQUE assessment with adaptive super-resolution enhancement improved prediction accuracy by 23 % for low-quality images. This improvement directly addresses findings by Yang et al. (2024), who identified image quality as a major limiting factor in smartphone-based soil analysis.

In terms of operational efficiency, the model processed samples in an average of 2.3 s, making it practical for field deployment, albeit marginally slower than regression-based alternatives. Its consistent performance across soil textures (RMSE variation < 0.05) further strengthens its applicability, contrasting with traditional models that exhibited up to threefold variability in texture-dependent performance (Gorthi et al., 2021a; Swetha et al., 2020). While promising, the system's reduced accuracy for extreme SOM values (>10 %) and its performance under uncontrolled lighting conditions and computational limitations remain areas for further investigation. Additionally, broader deployment will require attention to integration with farm management systems, user training, and considerations of digital literacy within target communities.

4.3. Methodological contributions and future directions

Our study introduces several methodological innovations that could have broader implications for digital soil sensing. The integration of BRISQUE assessment and adaptive super-resolution enhancement offers a refined strategy for ensuring measurement reliability under variable conditions. This framework could be adapted for other soil properties beyond SOM, potentially enabling comprehensive soil characterization from single image captures.

The similarity-based architecture, grounded in Triplet Loss, introduces a learning paradigm focused on relative comparisons rather than absolute regression mappings. This perspective opens up opportunities for transfer learning, where models trained in one geographic context may be adapted to others with minimal retraining. Given the strong generalization performance observed across diverse textures and environmental conditions, future research could explore leveraging learned feature embeddings for other soil-related prediction tasks. While our approach does not aim to replace laboratory methods, it offers a scalable, interpretable, and field-adaptable complement for high-frequency monitoring and precision agriculture applications. Smartphones, with their integrated sensors, embedded metadata, and

compatibility with portable calibration tools, offer a low-cost, practical alternative to hyperspectral systems. Unlike hyperspectral cameras, which are expensive and logistically demanding, smartphones enable real-time SOM estimation through adaptable color-correction routines, facilitating a transition from controlled laboratory conditions to in-field applications. Although field-acquired bare-soil images introduce greater variability, with further refinement and region-specific calibration, this system could enhance accessibility to reliable soil data, particularly in resource-limited agricultural settings.

5. Conclusions

This study contributes to digital soil analysis by developing and validating a similarity-based deep learning approach for SOM prediction using smartphone imagery, offering a new perspective within the field. By leveraging Triplet Loss networks and enhanced image processing techniques, the model achieved strong predictive performance and demonstrated robustness across soil textures and environmental conditions. These findings suggest that learning from relative relationships between samples offers improved generalization and reliability for field-based applications.

While the model showed consistent accuracy within common SOM ranges, further validation is needed for extreme values and across diverse geographic regions. The integration of image quality assessment and adaptive enhancement also supports more stable predictions under variable field conditions. Overall, this work advances the potential for accessible, smartphone-based soil analysis and contributes to sustainable agriculture by enabling rapid and reliable SOM monitoring. Future efforts should focus on expanding to other soil properties, supporting regional adaptation, and ensuring usability in diverse agricultural contexts.

CRediT authorship contribution statement

Mojtaba Naeimi: Writing – original draft. **Vishvam Porwal:** Methodology. **Stacey Scott:** Writing – review & editing. **Maja Krzic:** Writing – review & editing. **Prasad Daggupati:** Writing – review & editing. **Hiteshkumar Vasava:** Data curation. **Daniel Saurette:** Writing – review & editing. **Ayan Biswas:** Conceptualization. **Abhinandan Roul:** Data curation. **Asim Biswas:** Writing – review & editing.

Declaration of competing interest

The authors declare that they have no known competing financial interests or personal relationships that could have appeared to influence the work reported in this paper.

Data availability

Data will be made available on request.

References

- Aitkenhead, M., Cameron, C., Gaskin, G., Choisy, B., Coull, M., Black, H., 2018. Digital RGB photography and visible-range spectroscopy for soil composition analysis. *Geoderma* 313, 265–275. <https://doi.org/10.1016/j.geoderma.2017.11.020>.
- Aitkenhead, M., Donnelly, D., Coull, M., Gwatkin, R., 2016. *Estimating Soil Properties with a Mobile Phone*. Springer, Cham, pp. 89–110.
- Aitkenhead, M.J., Poggio, L., Wardell-Johnson, D., Coull, M.C., Rivington, M., Black, H.I. J., Yacob, G., Boke, S., Habte, M., 2020. Estimating soil properties from smartphone imagery in Ethiopia. *Comput. Electron. Agric.* 171, 105322. <https://doi.org/10.1016/J.COMPAG.2020.105322>.
- Asad, M.H., Odeoluwa, B.E., Bais, A., 2024. Mapping Soil Organic Matter under Field Conditions. *IEEE Transactions on AgriFood Electronics* 2 (1), 138–150. <https://doi.org/10.1109/TAFE.2024.3369995>.
- Azadnia, R., Jahanbakhshi, A., Rashidi, S., Khajehzadeh, M., 2022. Developing an automated monitoring system for fast and accurate prediction of soil texture using an image-based deep learning network and machine vision system. *Measurments* 190. <https://doi.org/10.1016/j.measurement.2021.110669>.

- Babalola, E.-O., Asad, M.H.H., Bais, A., 2023. Soil Surface Texture Classification using RGB Images acquired under Uncontrolled Field Conditions. *IEEE Access* 11, 67140–67155. <https://doi.org/10.1109/ACCESS.2023.3290907>.
- Cheng, G., Li, Z., Han, J., Yao, X., Guo, L., 2018. Exploring Hierarchical Convolutional Features for Hyperspectral image Classification. *IEEE Trans. Geosci. Remote Sens.* 56 (11), 6712–6722. <https://doi.org/10.1109/TGRS.2018.2841823>.
- Cheung, V., Rhodes, P.A., 2023. Uniform Color Spaces. In: *Handbook of Visual Display Technology*. Springer, Berlin Heidelberg, pp. 1–12.
- Fan, Y., Li, J., Guo, Y., Xie, L., Zhang, G., 2021. Digital image colorimetry on smartphone for chemical analysis: a review. *Measurments* 171. <https://doi.org/10.1016/j.measurement.2020.108829>.
- Fan, Z., Herrick, J., Saltzman, R., C. M.-S. S. S., & 2017, undefined., 2017. Measurement of soil color: a comparison between smartphone camera and the Munsell color charts. *Soil Sci. Soc. Am. J.* 81 (5), 1139–1146. <https://doi.org/10.2136/sssaj2017.01.0009>.
- Fu, Y., Taneja, P., Lin, S., Ji, W., Adamchuk, V., Daggupati, P., Biswas, A., 2020. Predicting soil organic matter from cellular phone images under varying soil moisture. *Geoderma* 361, 114020. <https://doi.org/10.1016/j.geoderma.2019.114020>.
- Gomez-Robledo, L., Lopez-Ruiz, N., Melgosa, M., Palma, A.J., Fermin Capitan-Vallvey, L., Sanchez-Maranon, M., 2013. Using the mobile phone as Munsell soil-colour sensor: an experiment under controlled illumination conditions. *Comput. Electron. Agric.* 99, 200–208. <https://doi.org/10.1016/j.compag.2013.10.002>.
- Gozukara, G., Hartemink, A.E., Zhang, Y., 2023. Illumination levels affect the prediction of soil organic carbon using smartphone-based digital images. *Comput. Electron. Agric.* 204, 107524. <https://doi.org/10.1016/J.COMPAG.2022.107524>.
- Hermanns, A., Beyer, L., Leibe, B., 2017. Defense of the Triplet loss. for Person Re-Identification.
- Inik, O., Inik, Ö., Öztaş, T., Demir, Y., Yüksel, A., 2023. Prediction of Soil Organic Matter with Deep Learning. *Arab. J. Sci. Eng.* 48 (8), 10227–10247. <https://doi.org/10.1007/S13369-022-07575-X/TABLES/11>.
- Kang, Y., Lee, J., Kim, J., Oh, T., 2024. Quantifying soil organic matter for sustainable agricultural land management with soil color and machine learning technique. *Agron. J.* 116 (3), 982–989. <https://doi.org/10.1002/agj2.21525>.
- Li, H., Ju, W., Song, Y., Cao, Y., Yang, W., Li, M., 2024. Soil organic matter content prediction based on two-branch convolutional neural network combining image and spectral features. *Comput. Electron. Agric.* 217, 108561. <https://doi.org/10.1016/j.compag.2023.108561>.
- Li, Y., Zhang, Y., Huang, X., Zhu, H., Ma, J., 2018. Large-Scale Remote Sensing image Retrieval by Deep Hashing Neural Networks. *IEEE Trans. Geosci. Remote Sens.* 56 (2), 950–965. <https://doi.org/10.1109/TGRS.2017.2756911>.
- Nazir, M.J., Li, G., Nazir, M.M., Zulfiqar, F., Siddique, K.H.M., Iqbal, B., Du, D., 2024. Harnessing soil carbon sequestration to address climate change challenges in agriculture. *Soil Tillage Res.* 237, 105959. <https://doi.org/10.1016/j.still.2023.105959>.
- Nodi, S.S., Paul, M., Robinson, N., Wang, L., Rehman, S., ur., 2023. Determination of Munsell Soil Colour using Smartphones. *Sensors* 23 (6). <https://doi.org/10.3390/S23063181>.
- Qiao, L., Wang, X., Smith, P., Fan, J., Lu, Y., Emmett, B., Li, R., Dorling, S., Chen, H., Liu, S., et al., 2022. Soil quality both increases crop production and improves resilience to climate change. *Nat. Clim. Chang.* 12 (6), 574–580. <https://doi.org/10.1038/s41558-022-01376-8>.
- Roy, S., Sangineto, E., Demir, B., Sebe, N., 2018. Deep Metric and Hash-Code Learning for Content-based Retrieval of Remote Sensing Images. In: IGARSS 2018–2018 IEEE International Geoscience and Remote Sensing Symposium, pp. 4539–4542. <https://doi.org/10.1109/IGARSS.2018.8518381>.
- Schroff, F., Kalenichenko, D., Philbin, J., 2015. FaceNet: a unified embedding for face recognition and clustering. *IEEE Conference on Computer Vision and Pattern Recognition (CVPR) 2015*, 815–823. <https://doi.org/10.1109/CVPR.2015.7298682>.
- Swetha, R.K., Bende, P., Singh, K., Gorthi, S., Biswas, A., Li, B., Weindorf, D.C., Chakraborty, S., 2020. Predicting soil texture from smartphone-captured digital images and an application. *Geoderma* 376, 114562. <https://doi.org/10.1016/j.geoderma.2020.114562>.
- Taneja, P., Vasava, H.K., Daggupati, P., Biswas, A., 2021. Multi-algorithm comparison to predict soil organic matter and soil moisture content from cell phone images. *Geoderma* 385, 114863. <https://doi.org/10.1016/j.geoderma.2020.114863>.
- Tobiszewski, M., Vakh, C., 2023. Analytical applications of smartphones for agricultural soil analysis. *Anal. Bioanal. Chem.* 415 (18), 3703–3715. <https://doi.org/10.1007/s00216-023-04558-1>.
- Waqas, M., Naseem, A., Humphries, U.W., Hlaing, P.T., Dechpichai, P., Wangwongchai, A., 2025. Applications of machine learning and deep learning in agriculture: a comprehensive review. *Green Technol. Sustainability* 3 (3), 100199. <https://doi.org/10.1016/j.grets.2025.100199>.
- Yan, Y., Li, B., Rossel, R.V., Sun, F., Huang, Y., Shen, C., Shi, Z., Ji, W., 2023. Optimal soil organic matter mapping using an ensemble model incorporating moderate resolution imaging spectroradiometer, portable X-ray fluorescence, and visible near-infrared data. *Comput. Electron. Agric.* 210, 107885. <https://doi.org/10.1016/j.compag.2023.107885>.
- Yang, J., Shen, F., Wang, T., Luo, M., Li, N., Que, S., 2021. Effect of smart phone cameras on color-based prediction of soil organic matter content. *Geoderma* 402, 115365. <https://doi.org/10.1016/j.GEODERMA.2021.115365>.
- Yang, J., Wang, T., Que, S., Li, Z., Liang, Y., Wei, Y., Li, N., Xu, Z., 2024. Effect of colour calibration on the prediction of soil organic matter content based on original soil images obtained from smartphones under different lighting conditions. *Soil Tillage Res.* 238, 106018. <https://doi.org/10.1016/j.still.2024.106018>.
- Zeraatpisheh, M., Garosi, Y., Owliaie, H.R., Ayoubi, S., Taghizadeh-Mehrjardi, R., Scholten, T., Xu, M., 2022. Improving the spatial prediction of soil organic carbon using environmental covariates selection: a comparison of a group of environmental covariates. *Catena* 208, 105723. <https://doi.org/10.1016/j.catena.2021.105723>.
- Zhao, M., Sheng, H., Yang, D., Wang, S., Cong, R., Cui, Z., Chen, R., Wang, T., Wang, S., Huang, Y., Shen, J., 2024. A survey for light field super-resolution. *High-Confid. Comput.* 4 (1), 100206. <https://doi.org/10.1016/j.hcc.2024.100206>.
- Zurek, M., Hebinck, A., Selomane, O., 2022. Climate change and the urgency to transform food systems. *Science* 376 (6600), 1416–1421. <https://doi.org/10.1126/science.abo2364>.